# Terrestrial biodiversity threatened by increasing global aridity velocity under high level warming

Hao Shi[a,b], Hanqin Tian[a,1], Stefan Lange[c], Jia Yang[a,d], Shufen Pan[a], Bojie Fu[b], Christopher P.O. Reyer[c]

[a]International Center for Climate and Global Change Research, School of Forestry and Wildlife Sciences, Auburn University, AL 36849, USA
[b]State Key Laboratory of Urban and Regional Ecology, Research Center for Eco-Environmental Sciences, Chinese Academy of Sciences, Beijing 100085, China.
[c]Potsdam Institute for Climate Impact Research (PIK), Member of the Leibniz Association, P.O. Box 60 12 03, 14412 Potsdam, Germany
[d]Department of Forestry, Mississippi State University, Mississippi State, Mississippi, USA

[1]Corresponding author: Hanqin Tian (tianhan@auburn.edu)

**Keywords:** Terrestrial biodiversity, climate velocity, aridification, global warming

## Abstract

Global aridification is projected to intensify. Yet our knowledge of its potential impacts on species ranges remains limited. Here, we investigate global aridity velocity and its overlap with three sectors (natural protected areas, agricultural and urban areas) and terrestrial biodiversity in historical (1979-2016) and future periods (2050-2099), with and without considering vegetation physiological response to rising $CO_2$. Both agricultural and urban areas showed a mean drying velocity in history, although the concurrent global aridity velocity was on average +0.05/+0.20 km $yr^{-1}$ (no $CO_2$ effects/with $CO_2$ effects; "+" denoting wetting). Moreover, in drylands the shifts of vegetation greenness isolines were found to be significantly coupled with the tracks of aridity velocity. In future, the aridity velocity in natural protected areas is projected to change from wetting to drying across RCP2.6, RCP6.0 and RCP8.5 scenarios. When accounting for spatial distribution of terrestrial taxa (including plants, mammals, birds and amphibians), the global aridity velocity would be -0.15/-0.02 km $yr^{-1}$ ("-" denoting drying; historical), -0.12/-0.15 km $yr^{-1}$ (RCP2.6), -0.36/-0.10 km $yr^{-1}$ (RCP6.0) and -0.75/-0.29 km $yr^{-1}$ (RCP8.5), with amphibians particularly negatively impacted. Under all scenarios, aridity velocity shows much higher multi-directionality than temperature velocity, which is mainly poleward. These results suggest that aridification risks may significantly influence the distribution of terrestrial species besides warming impacts and further impact the effectiveness of current protected areas in future, especially under RCP8.5, which best matches historical $CO_2$ emissions (1).


## Significance

Under climate change, a point on a map needs to move in some speed and direction to maintain its current climate niche. We calculated the speeds and directions of aridity shifts across the globe to approximate species migration in natural-human systems driven by changes in water availability. We found historically the aridity shifts had driven migration of vegetation greenness isolines in multiple regions. Most importantly, global drying would be accelerated for terrestrial taxa without mitigation actions. This would leave some species unable to adapt quickly enough, especially amphibians, which will suffer the largest aridification speed against plants, birds and mammals. These findings suggest strong climate mitigation actions are required for the benefit of both terrestrial biodiversity and human well-being.

## Introduction

There is general agreement that climate warming will be one of the greatest threats to ecosystem functioning in multiple ways and have substantial impacts on agriculture and human health (2, 3). As a response to warming, precipitation will also increase but with large spatial heterogeneity (4). The reshuffling of temperature and precipitation will lead to shift of current or emergence of new aridity regimes. These changes are predicted to result in complicated biological consequences as aridity plays an important role in controlling ecosystem dynamics and biogeochemical cycling (5-8). This is true even in humid regions as the temporal distribution of water availability is usually not uniform and species have adapted to high water availability. Take tropical ecosystems as an instance, even modest changes in dry-season length can increase tropical tree mortality (9) and longer dry seasons can change the population growth rates and structure of tropical bird

communities (10). Persistent drying would degrade tropical forest canopies (11) and further have detrimental effects on biodiversity (12), resulting in functional, taxonomic and phylogenetic homogenization (13).

Many studies have reported warming impacts on species ranges (14, 15), such as their poleward and uphill shifts. Yet, how aridity changes will drive species shifts has not been well addressed. Moreover, most previous studies ignored species like different varieties of crops and urban trees in human managed systems. To date, it is still a grand challenge to assess the shift rate of each of major species in response to climate forcing, as species-specific migration models are usually built upon very limited observations in the current climate conditions (16, 17) . Therefore, we use the generic but ecologically relevant local climate velocity to approximate species migration rates (15, 18), which, through merging spatial and temporal gradients, describes the moving speed and direction required by a point to maintain its current climate domain. A number of studies have shown a remarkable correlation between observed terrestrial or marine species shifts and the velocity of climate warming (19-21). Since ecosystems are individually or jointly controlled by temperature and water availability, it is expected that ecosystems will also be impacted by the aridity velocity (derived from aridity index, the ratio of precipitation over potential evapotranspiration).

In this study we evaluate how aridity velocity changes from historical (1979-2016) to future periods, using the aridity index based on the FAO reference crop potential evapotranspiration model (AI_RC) and one of its variants considering vegetation physiological responses to elevated $CO_2$ (AI_$CO_2$) developed by Yang *et al.* (22). Following Loarie *et al.* (15) and Diffenbaugh and Field (14), we focus on a future period (2050-2099) under three Representative Concentration Pathways (RCP2.6, RCP6.0 and RCP8.5) rather than the whole century as climate change is more linear within a limited time window, facilitating the assumption of linear trends in estimating climate velocity. Meanwhile, we also calculate the migration of isolines of vegetation greenness using satellite observations during 1982-2015 to compare with the concurrent aridity velocity. Furthermore, we stack the projected aridity velocity to the global distributions of terrestrial vertebrates and plants to identify areas and taxa of high aridification risks. Because aridity is a nonlinear function of multiple climatic variables that may have complex interactions, it is hypothesized that aridity velocity would show non-uniform change under different RCPs.

## Results

Our results show that during 1979-2016 aridity velocities based on AI_RC and AI_$CO_2$ showed minor difference in either speed or direction (Figs. 1*A* and 1*B*). Aridity velocity exhibited wetting patterns in Sahel Africa, southwestern Africa, most parts of Asia, and Australia, but drying patterns in most of North and South America, Europe, Middle East, and west Russia (Figs. 1*A* and 1*B*). In contrast, the changes in the concurrent temperature velocity were more homogeneous (Fig. 1*C*). The directions of aridity and temperature velocities showed obvious differences that aridity velocity (for both AI_RC and AI_$CO_2$) was more multi-directional at the global scale (*SI Appendix*, Figs. S1*A* and S1*B*) whereas temperature velocity was generally poleward (*SI Appendix*, Fig. S1*C*). But at the regional scale aridity velocity showed one uniform direction in some areas, such as in central U.S. (eastward), Sahel Africa (northward), and northwestern Australia (southward, *SI Appendix*, Figs. S1*A* and S1*B*). In future, the aridity velocity tends to be more southward and eastward (*SI Appendix*, Fig. S1). We also compared the aridity velocities (for AI_RC) derived from two different historical climate datasets, i.e., EWEMBI and CRUNCEP, and found they were

generally consistent in the spatial patterns (*SI Appendix*, Fig. S2) and had comparable global mean aridity velocity (+0.05 km $yr^{-1}$ *vs.* +0.01 km $yr^{-1}$), with major differences located in east North America and east Australia (*SI Appendix*, Fig. S2).

<Figure 1 here>

Aridity velocities under RCP2.6 generally show a weaker magnitude than those in history, but there would be more areas with drying velocities in the Southern Hemisphere (Figs. 1*D* and 1*E*). Particularly in Australia, the historical wetting velocities would turn to drying velocities (Figs. 1*D* and 1*E*) directing to coastlines (*SI Appendix*, Figs. S1*D* and S1*E*). Higher warming under RCP6.0 would greatly influence the spatial patterns of aridity velocities in the Northern Hemisphere (Figs. S1*G* and S1*H*). The most obvious changes occur in east North America, Europe west and east Siberia with the sign of aridity velocity reversed (Figs. 1*G* and 1*H*). Further warming under RCP8.5 results in similar spatial patterns of aridity velocities to those under RCP6.0 but with larger speeds, notably in North America, Europe, east Siberia, South America and southern Africa (Figs. 1*J* and 1*K*). Across all the three RCP scenarios, the largest uncertainty (in standard deviation) of aridity velocity among different climate projections occurs in northern high latitudes, Amazon and Australia (*SI Appendix*, Fig. S4). The spatial patterns of uncertainty in future aridity velocity are similar to those of future temperature velocity (*SI Appendix*, Fig. S3) and both are related to topography (*SI Appendix*, Fig. S4 and Discussion S1).

To validate whether the estimated aridity velocities are indicative of vegetation shifts, we calculated isolines of multi-year mean annual vegetation greenness during 1982-1986 and 2011-2015, respectively, using the AVHRR NDVI3g v1 dataset. Northern Australia, Sahel and southern Africa (Fig. 2) were particularly taken as examples, because ecosystems in these regions are water-dominated and have relatively flat landscapes and low intensity of human activities, such as irrigation, grazing, wood harvest and deforestation (*SI Appendix*, Figs. S5-S8), which are particularly beneficial for detecting long-term expansion or contraction of vegetation ranges induced by aridity changes. The migration distances (*SI Appendix*, Method S1) of NDVI isolines in the three regions were all significantly correlated with the concurrent aridity velocities (Fig. 2). Moreover, we also used the AVHRR vegetation continuous fields (VCF) data to investigate whether the isolines of herbaceous fractions migrated following aridity velocity. The results show that herbaceous VCF was significantly coupled with aridity velocity in both Sahel ($r = 0.35$ and $p < 0.001$; *SI Appendix*, Fig. S9*B*) and southern Africa ($r = 0.73$ and $p < 0.001$; *SI Appendix*, Fig. S9*C*), except in northern Australia. The reason lies in that the responses of vegetation greenness and vegetation composition to drying or wetting are not always synchronous. In northern Australia, as wetting during 1982-2015, NDVI generally increased but herbaceous fraction decreased in a large extent (Fig. 2A and *SI Appendix*, Fig. S9*A*). Zhang *et al.* (23) also reported this phenomenon and found the altered rainfall climatology characterized by the increase of heavy rainfall favored woody vegetation in its competition with herbaceous vegetation.

<Figure 2 here>

Across the globe, aridity velocity basically obeys a Gaussian distribution, with the mean speed of AI_RC based aridity velocity from +0.05 km $yr^{-1}$ in history changing to a drying speed of -0.06 km $yr^{-1}$ under RCP2.6, -0.19 km $yr^{-1}$ under RCP6.0 and -0.42 km $yr^{-1}$ under RCP8.5, respectively (Fig. 3A). The corresponding global mean speed of AI_$CO_2$ based aridity velocity is +0.20 km $yr^{-1}$, -0.11 km $yr^{-1}$, +0.13 km $yr^{-1}$, and +0.15 km $yr^{-1}$, respectively (Fig. 3E). Beyond the global average aridity velocities are their specific changes in protected areas, agricultural areas, and urban

areas. Protection areas have covered 4~25% of 14 major terrestrial biomes since 2009 (24) and contain high levels of endemism and small-ranged species. Thus, the changes of aridity velocity therein are more meaningful than the global average. Our analysis shows the aridity velocity in protected areas would change from historical +0.22 km $yr^{-1}$/+0.36 km $yr^{-1}$ (no $CO_2$ effects/with $CO_2$ effects) to -0.72 km $yr^{-1}$/-0.24 km $yr^{-1}$ under RCP8.5 (Fig. 3). The aridity velocity also manifests a significant change from historical -0.56 km $yr^{-1}$/-0.41 km $yr^{-1}$ to -0.65 km $yr^{-1}$/-0.13 km $yr^{-1}$ under RCP8.5 in agricultural areas (Fig. 3). In urban areas, the corresponding values are changing from -0.66 km $yr^{-1}$/-0.52 km $yr^{-1}$ to -0.77 km $yr^{-1}$/-0.24 km $yr^{-1}$ (Fig. 3). Of 18 socio-economic regions (*SI Appendix*, Fig. S10), protected areas in Brazil, Southern Africa, Central America and Oceania, agricultural areas in Brazil, Europe, Southern Africa and Central America, and urban areas in Southern Africa, Europe, and Brazil would experience the largest drying velocity under RCP8.5 (*SI Appendix*, Fig. S11 and Discussion S2).

<Figure 3 here>

Since most wetting velocities occur in high latitudes under RCP6.0 and RCP8.5 (Fig. 1) while most terrestrial species live in low- and high-latitudes, it is necessary to consider the spatial pattern of terrestrial biodiversity to evaluate potential impacts of changing aridity velocity. When accounting for richness distribution of terrestrial taxa (including amphibians, birds, mammals and plants), the global mean aridity velocity changes from historical -0.15 km $yr^{-1}$ to -0.12 km $yr^{-1}$, -0.36 km $yr^{-1}$ and -0.75 km $yr^{-1}$ based on AI_RC or from historical -0.02 km $yr^{-1}$ to -0.15 km $yr^{-1}$, -0.10 km $yr^{-1}$ and -0.29 km $yr^{-1}$ based on AI_$CO_2$, respectively, under the three RCPs. Across all scenarios, taxa in arid regions would experience the largest change in aridity velocity from historical wetting to future drying (Fig. 4). Taxa in humid regions, which have the highest species richness, would experience the largest drying velocities under RCP8.5 (Fig. 4). Of all taxa, amphibians are projected to be most negatively impacted, particularly those in semi-arid, semi-humid and humid regions under RCP8.5, which tracks closely cumulative $CO_2$ emissions until now (1).

<Figure 4 here>

## Discussion

The selected dryness metric is of central importance for aridity projection. AI_RC is questioned about overestimation of future dryness as it lacks description of vegetation physiological response to increasing $CO_2$ (24, 25). AI_$CO_2$ could reproduce CMIP5 projected runoff using the offline Budyko model over most of the globe through water saving effects of elevated $CO_2$ (22). But it must be noted that such water-saving effects are not always persistent. For example, Ukkola *et al.* (26) reported that elevated $CO_2$ lead to vegetation greening (through $CO_2$ fertilization effects) and more water consumption in sub-humid and semi-arid basins but nonsignificant changes in NDVI and reductions in evapotranspiration in wet and arid basins across Australia during 1982-2010. Shimono *et al.* (27) also found that canopy evapotranspiration rate showed much lower responsiveness than stomatal conductance to open-air $CO_2$ elevation in rice. These observations mean that our original AI_RC formulation is still a reasonable approach in reflecting aridity changes even in a world of increasing $CO_2$ concentration. Therefore, AI_RC and AI_$CO_2$ are simultaneously used in this study to represent a spectrum of possible dryness change in future.

Before this effort, little research has focused on the impacts of water availability on species shifts except few examples (3, 28). However, these exceptional studies still used precipitation to indicate water availability, which is projected to have an increasing trend opposite to aridity (*SI Appendix*, Fig. S12). Therefore, previous estimates, based on temperature only or even taking precipitation into account, when assessing threats of climate change to species shifts and the associated complexity could be underestimated. From this perspective, our results can provide complemental references for guiding allocation of limited conservation and adaptation resources.

For nature conservation, our estimated aridity velocity can help identify priority regions where species shifts are influenced by water availability, particularly at the leading edges of species range and for narrow-ranged species (16). In the identified hotspot areas, conservation actions may focus on monitoring of immigration or emigration of species and devote to mitigating other disturbances to aid indigenous species to adapt (16). A more specific example is that Malhi *et al.* (29) recommended to keep the core northwest Amazon intact as a biological refuge as it hosts the highest biodiversity and was expected to be the most resistant to climate drying in Amazon based on previous mid-range (A1B) emission scenarios. Our analysis, however, shows the northwest Amazon is also projected to experience considerable drying under high emission scenarios (Fig. 1), implying the imperative requirement for conservation actions to mitigate negative impacts of other factors in this area, such as reducing deforestation and controlling fires. Moreover, our results show that along coastal areas aridity velocities may point to coastlines (e.g., Australia; *SI Appendix*, Fig. S1), which means many coastal niches could not find their climate analogs due to the ocean barrier. In addition, our methodology and results can help the design of protected area networks and ecological corridors to connect large nature reserves across a continent. An excellent effort has been conducted in informing the design of the North American protected area network (28). Batllori *et al.* (28) found the majority of protected areas in North America might be exposed to high climate velocity and the nearest climatic analogs are outside the current network of protected areas. Thus, they suggest that conservation plan needs to take advantage of these unprotected climate refuges and avoid additional threats there beyond climate change.

Under all the three RCPs, some regions are projected to experience large aridification risks for crop species and food production, particularly in rain-fed areas like Southern Africa and Brazil (*SI Appendix*, Fig. S13). Unfortunately, there has been much less research on migration of crop species, pasture, weeds and insects, etc. in responding to climate velocity. But limited evidence shows that crop wild relatives could lose up to 91% of their distribution range in protected areas even with full dispersal under RCP8.5, which is 50% higher than that under RCP2.6 (30). Yield loss risk for four major crops (wheat, maize, rice and soybeans) has also been reported across moderate to exceptional drought conditions, particularly in the US, and it could be amplified by high temperature (31). A very recent study (32) also shows that changes in growing season temperature had driven migration of the harvested areas of rainfed maize, wheat, rice and soybean during 1973-2012. For species that are highly sensitive to climate change, the situation could be more severe. Take coffee for instance, its distribution area is predicted to decrease by about 50% across RCPs, and the new suitable habitats are far from the current plantation locations and currently occupied by forests (33). In addition, insects like locusts generally thrive in warm and dry conditions (34), and their dispersal tracking aridity velocity will no doubt deteriorate food production. Therefore, as population increases, this might drive agricultural area, irrigated fraction or fertilizer application to increase to compensate for yield loss, in which case securing food supply would inevitably conflict with the exacerbated aridity velocity predicted here and environmental externalities of

crop production increase. To cope with this situation, crop drought traits and planting structure should be improved.

The drying velocities in urban areas (e.g., in Central America and Europe; *SI Appendix*, Fig. S11) could greatly influence plants, animals and human health there. Since urban landscapes are usually highly fragmented, urban trees or forests are unlikely to escape from increased aridity through spatial shifts. Those tree species that are not suited to low water availability would have to be substituted by drought-tolerant species or irrigated more often, which will increase maintenance cost. Animals that depend on original trees or forests may suffer from water scarcity and loss of feeding source or shelters, and it is difficult for them to cross the urban barrier to migrate elsewhere. The possible decreased benefits provided by urban trees or forests, such as aesthetic value, tree shade, and air and water quality, are associated with health problems (35-37). The efforts for enabling urban areas to adapt to the drying aridity velocity may involve high cost, for example, infrastructure upgrade fee.

It is important to note that climate velocity has its own caveats. Brito-Morales *et al.* (16) summarized that climate velocity does not include biological information and may be misleading due to its fractional nature (i.e., ratio of a temporal trend over a spatial gradient). In our analysis, we also noticed that there existed some aridity velocities of abnormally large magnitudes compared to their neighboring counterparts (Fig. 2) and the migration of vegetation herbaceous fraction does not always track climate velocity (*SI Appendix*, Fig. S9*A*). Therefore, interpretation of changes in climate velocity and their impacts on biodiversity needs carefulness and fully considering the exposure, sensitivity, and vulnerability of individual species to climate change, together with their adaptive capacities (38). However, the magnitude and direction of climate velocity are still indicative in reflecting expected shifts of species ranges.

The spatial and temporal resolutions used in this analysis are also a potential source of uncertainty in estimating aridity velocity and its impacts on biodiversity. The half-degree climate data doesn't capture fine-scale topographic differences in climate and may underestimate climate heterogeneity, especially for urban or mountain areas. Therefore, our results may underestimate drying velocity in urban areas, as cities usually have higher temperature than neighboring areas due to the heat island effect. Meanwhile, the annual time step can obscure the signal of intra-annual variations in water availability, which may have considerable impacts on changes in ecosystem production and composition (9, 10). However, urban extent data and parameters and climate data at the half-degree or similar resolutions have been employed to examine interaction between urban expansion and climate warming (39-41), providing a certain confidence for employing climate data of the half-degree resolution. Moreover, consideration of long-term changes in aridity velocity of different seasons would be much more complex as different species or biological processes have different matching temporal windows (16). Therefore, for this study we still focus on the annual changes in aridity velocity to keep it simple and leave seasonal climate velocity in future research, which could be another great story to explore.

## Materials and Methods

**Aridity index.** We used the aridity index, the ratio of precipitation to potential evapotranspiration (PET), to indicate aridity. PET is estimated through the FAO reference method (42; PET_RC) and one of its variants considering surface response to elevated $CO_2$ (22; PET_$CO_2$), which are parameterized, respectively, as:

$$PET\_RC = \frac{0.408\Delta R_n^* + \gamma \frac{900}{T+273} uD}{\Delta + \gamma(1+0.34u)} \quad (1)$$

$$PET\_CO_2 = \frac{0.408\Delta R_n^* + \gamma \frac{900}{T+273} uD}{\Delta + \gamma(1+u(0.34+2.4\times10^{-4}([CO_2]-300)))} \quad (2)$$

where $\Delta$ (Pa $K^{-1}$) is the gradient of saturation vapor pressure against temperature, $R_n^*$ (MJ $m^{-2}$ $d^{-1}$) is the surface available net radiation, $\gamma$ (Pa $K^{-1}$) is the psychrometric constant, $T$ (°C) is the air temperature at 2 m height, $D$ (Pa) is air vapor pressure deficit, $u$ (m $s^{-1}$) is the wind speed at 2 m height, and [$CO_2$] is the atmospheric $CO_2$ concentration. These PET models take into account changes in available energy, atmospheric humidity and wind speed, and thus can give more realistic estimation of PET than those methods only considering changes in temperature. During 1979-2016, the daily EWEMBI (40) (E2OBS, WFDEI and ERAI data Merged and Bias-corrected for ISIMIP) and CRU-NCEP v8.0 dataset (both at a 0.5˚ resolution), including surface air temperature, precipitation, surface wind speed, atmospheric pressure, specific humidity and downward shortwave radiation, were used to estimate daily PET, which then was aggregated to the annual time-scale to derive annual aridity index. For the future period, according to the RCP and daily data availability, we used outputs of nine global climate models (including CSIRO-Mk3.6.0, GFDL-CM3, GFDL-ESM2M, HadGEM2-ES, IPSL-CM5A-LR, MIROC5, MIROC-ESM-CHEM, MRI-CGCM3, and NorESM1-M) to derive aridity index under RCP2.6, RCP6.0 and RCP8.5. These models can well represent the CMIP5 ensemble in terms of equilibrium climate sensitivity (3.55 °C *vs.* 3.22 °C) and transient climate response (1.81 °C *vs.* 1.84 °C; *SI Appendix*, Fig. S14). The climate projections have been bias-corrected at a daily timestep and downscaled referring to EWEMBI. The annul aridity velocities of each of the nine models and the ensemble mean were adopted to represent the future aridity velocity under the three RCP scenarios and the corresponding standard deviation.

**Aridity velocity.** The local climate velocity approach (15) was used to calculate the moving speed and direction of aridity. Originally, the approach was introduced to estimate the local migration velocity of species to maintain their favorable temperatures as global warming shifts temperature isolines in space. Here we apply the approach to both AI_RC and AI_$CO_2$ instead of to temperature. Specifically, climate velocity is calculated as $\frac{Temporalslope}{Spatialgradient}$. The temporal slope is derived by linearly regressing the annual time series in a grid cell. The spatial gradient is determined from a 3×3 window of mean climate during 1979-2016 using the cell-neighborhood method. The direction of climate velocity depends on both the sign of the temporal slope and the direction of the spatial gradient. The value of a velocity direction ranges from 0˚ to 360˚, with 180˚ towards the straight south. Assuming the aridity velocity has a positive value of 1 km $yr^{-1}$ and a spatial gradient direction of 90˚ during 2017-2050 and the reference mean climate is calculated from 1979-2016, the mean aridity in a specific grid cell during 1979-2016 could be found 33 km to the east by the year 2050, where it has a drier climate than the grid during 1979-2016. In our analysis, the reference period was set to 1979-2016 to calculate the climatology of aridity index to derive the spatial gradient.

**Land use, region classification, vegetation greenness, herbaceous cover fraction and biodiversity richness.** The protected areas (*SI Appendix*, Fig. S8) were compiled from the World Database on Protected Areas (WDPA, https://protectedplanet.net/), April 2019. The WDPA is the most comprehensive database of terrestrial and marine protected areas, jointly developed by UN Environment and the International Union for Conservation of Nature. There are now over 220,000 protected areas and only terrestrial ones are used here. The agricultural areas (including crops and pastures), urban areas and irrigation fractions in 2018 (*SI Appendix*, Fig. S13) were from the LUH2 v2h (land use harmonization, http://luh.umd.edu) data, which has a spatial resolution of 0.25˚×0.25˚ and an annual time-step. The region classification is shown in supplemental material (*SI Appendix*, Fig. S10). The AVHRR (Advanced Very High Resolution Radiometer) GIMMS (Global Inventory Monitoring and Modeling System) Normalized Difference Vegetation Index (NDVI) data (NDVI3g.v1) in 1982-1986 and 2011-2015 was resampled from 1 km to 0.5˚ to show the spatial shifts of vegetation greenness isolines. The AVHRR vegetation continuous fields (VCF) data (https://lpdaac.usgs.gov/products/vcf5kyrv001/) was also resampled from 0.05˚ to 0.5˚ to identify the spatial shifts of herbaceous fraction isolines. The plant biodiversity data was developed by combining spatially explicit models and estimates for native species loss and gains (43) and was achieved at http://ecotope.org/anthromes/biodiversity/plants/data/. The richness data for amphibians, birds, and mammals were mapped based on >21,000 species and at a spatial grain of 10×10 km (44) and available at https://biodiversitymapping.org/wordpress/index.php/home/.

## Acknowledgments and Data

This study has been supported by National Science Foundation (grant no. 1903722, 243232 and 1922687) and National Key R&D Program of China (No. 2017YFA0604700), SKLURE Grant (SKLURE2017-1-6). The ISIMIP research was supported in part by the German Federal Ministry of Education and Research (BMBF, grant no. 01LS1201A2 and 01LS1711A). This work also has received funding from the European Union's Horizon 2020 research and innovation programme under grant agreement no. 641816 "Coordinated Research in Earth Systems and Climate: Experiments, kNowledge, Dissemination and Outreach" (CRESCENDO) and under grant agreement 821010 "Cascading climate risks: towards adaptive and resilient European societies" (CASCADES); The CRU-NCEP data are freely available at https://vesg.ipsl.upmc.fr/thredds/catalog/work/p529viov/cruncep/V8_1901_2016/catalog.html. The bias-corrected GCMs outputs can be accessed from ISIMIP data portal (https://www.isimip.org/) upon request.

## References


1. C. R. Schwalm, S. Glendon, P. B. Duffy, RCP8.5 tracks cumulative $CO_2$ emissions. *Proceedings of the National Academy of Sciences* **117**, 19656-19657 (2020).
2. N. S. Diffenbaugh, D. L. Swain, D. Touma, Anthropogenic warming has increased drought risk in California. *Proceedings of the National Academy of Sciences* **112**, 3931-3936 (2015).
3. J. VanDerWal *et al.*, Focus on poleward shifts in species distribution underestimates the fingerprint of climate change. *Nature Climate Change* **3**, 239 (2012).
4. A. G. Pendergrass, D. L. Hartmann, The atmospheric energy constraint on global-mean precipitation change. *Journal of Climate* **27**, 757-768 (2014).
5. J. Bai *et al.*, Satellite-observed vegetation stability in response to changes in climate and total water storage in Central Asia. *Science of The Total Environment* **659**, 862-871 (2019).
6. M. Delgado-Baquerizo *et al.*, Decoupling of soil nutrient cycles as a function of aridity in global drylands. *Nature* **502**, 672 (2013).
7. C. Wang *et al.*, Aridity threshold in controlling ecosystem nitrogen cycling in arid and semi-arid grasslands. *Nature Communications* **5**, 4799 (2014).
8. J. Yang *et al.*, Amazon drought and forest response: Largely reduced forest photosynthesis but slightly increased canopy greenness during the extreme drought of 2015/2016. *Global change biology* **24**, 1919-1934 (2018).
9. N. McDowell *et al.*, Drivers and mechanisms of tree mortality in moist tropical forests. *New Phytologist* **219**, 851-869 (2018).
10. J. D. Brawn, T. J. Benson, M. Stager, N. D. Sly, C. E. Tarwater, Impacts of changing rainfall regime on the demography of tropical birds. *Nature Climate Change* **7**, 133-136 (2017).
11. T. Hilker *et al.*, Vegetation dynamics and rainfall sensitivity of the Amazon. *Proceedings of the National Academy of Sciences* **111**, 16041-16046 (2014).
12. L. Gibson *et al.*, Primary forests are irreplaceable for sustaining tropical biodiversity. *Nature* **478**, 378-381 (2011).
13. J. Aguirre-Gutiérrez *et al.*, Long-term droughts may drive drier tropical forests towards increased functional, taxonomic and phylogenetic homogeneity. *Nature communications* **11**, 1-10 (2020).
14. N. S. Diffenbaugh, C. B. Field, Changes in Ecologically Critical Terrestrial Climate Conditions. *Science* **341**, 486-492 (2013).
15. S. R. Loarie *et al.*, The velocity of climate change. *Nature* **462**, 1052 (2009).
16. I. Brito-Morales *et al.*, Climate velocity can inform conservation in a warming world. *Trends in ecology & evolution* **33**, 441-457 (2018).
17. A. Ordonez, J. W. Williams, Projected climate reshuffling based on multivariate climate-availability, climate-analog, and climate-velocity analyses: implications for community disaggregation. *Climatic Change* **119**, 659-675 (2013).
18. M. T. Burrows *et al.*, Geographical limits to species-range shifts are suggested by climate velocity. *Nature* **507**, 492 (2014).
19. I.-C. Chen, J. K. Hill, R. Ohlemüller, D. B. Roy, C. D. Thomas, Rapid range shifts of species associated with high levels of climate warming. *Science* **333**, 1024-1026 (2011).
20. M. L. Pinsky, B. Worm, M. J. Fogarty, J. L. Sarmiento, S. A. Levin, Marine taxa track local climate velocities. *Science* **341**, 1239-1242 (2013).
21. J. M. Sunday *et al.*, Species traits and climate velocity explain geographic range shifts in an ocean-warming hotspot. *Ecology letters* **18**, 944-953 (2015).

22. Y. Yang, M. L. Roderick, S. Zhang, T. R. McVicar, R. J. Donohue, Hydrologic implications of vegetation response to elevated $CO_2$ in climate projections. *Nature Climate Change* **9**, 44-48 (2019).
23. W. Zhang *et al.*, Ecosystem structural changes controlled by altered rainfall climatology in tropical savannas. *Nature communications* **10**, 1-7 (2019).
24. A. Berg, K. A. McColl, No projected global drylands expansion under greenhouse warming. *Nature Climate Change* **11**, 331-337 (2021).
25. T. F. Keenan, X. Luo, Y. Zhang, S. Zhou, Ecosystem aridity and atmospheric $CO_2$. *Science* **368**, 251-252 (2020).
26. A. M. Ukkola *et al.*, Reduced streamflow in water-stressed climates consistent with CO2 effects on vegetation. *Nature Climate Change* **6**, 75-78 (2016).
27. H. Shimono, H. Nakamura, T. Hasegawa, M. Okada, Lower responsiveness of canopy evapotranspiration rate than of leaf stomatal conductance to open-air CO2 elevation in rice. *Global change biology* **19**, 2444-2453 (2013).
28. E. Batllori, M.-A. Parisien, S. A. Parks, M. A. Moritz, C. Miller, Potential relocation of climatic environments suggests high rates of climate displacement within the North American protection network. *Global Change Biology* **23**, 3219-3230 (2017).
29. Y. Malhi *et al.*, Climate change, deforestation, and the fate of the Amazon. *science* **319**, 169-172 (2008).
30. J. Aguirre-Gutiérrez, R. van Treuren, R. Hoekstra, T. J. L. van Hintum, Crop wild relatives range shifts and conservation in Europe under climate change. *Diversity and Distributions* **23**, 739-750 (2017).
31. G. Leng, J. Hall, Crop yield sensitivity of global major agricultural countries to droughts and the projected changes in the future. *Science of The Total Environment* **654**, 811-821 (2019).
32. L. L. Sloat *et al.*, Climate adaptation by crop migration. *Nature communications* **11**, 1-9 (2020).
33. C. Bunn, P. Läderach, O. Ovalle Rivera, D. Kirschke, A bitter cup: climate change profile of global production of Arabica and Robusta coffee. *Climatic Change* **129**, 89-101 (2015).
34. A. Maxmen, Crop pests: Under attack. *Nature* **501**, S15 (2013).
35. A. F. Taylor, F. E. Kuo, W. C. Sullivan, Views of Nature and self-discipline: evidence from inner city children. *Journal of Environmental Psychology* **22**, 49-63 (2002).
36. R. Ulrich, View through a window may influence recovery from surgery. *Science* **224**, 420-421 (1984).
37. Y. You, S. Pan, Urban Vegetation Slows Down the Spread of Coronavirus Disease (COVID-19) in the United States. *Geophysical Research Letters* **47**, e2020GL089286 (2020).
38. T. P. Dawson, S. T. Jackson, J. I. House, I. C. Prentice, G. M. Mace, Beyond predictions: biodiversity conservation in a changing climate. *science* **332**, 53-58 (2011).
39. K. Huang, X. Li, X. Liu, K. C. Seto, Projecting global urban land expansion and heat island intensification through 2050. *Environmental Research Letters* **14**, 114037 (2019).
40. E. S. Krayenhoff, M. Moustaoui, A. M. Broadbent, V. Gupta, M. Georgescu, Diurnal interaction between urban expansion, climate change and adaptation in US cities. *Nature Climate Change* **8**, 1097-1103 (2018).

41. K. W. Oleson, G. B. Bonan, J. Feddema, T. Jackson, An examination of urban heat island characteristics in a global climate model. *International Journal of Climatology* **31**, 1848-1865 (2011).
42. R. G. Allen, L. S. Pereira, D. Raes, M. Smith, Crop evapotranspiration-Guidelines for computing crop water requirements-FAO Irrigation and drainage paper 56. *FAO, Rome* **300**, D05109 (1998).
43. E. C. Ellis, E. C. Antill, H. Kreft, All Is not loss: Plant biodiversity in the Anthropocene. *PLOS ONE* **7**, e30535 (2012).
44. C. N. Jenkins, S. L. Pimm, L. N. Joppa, Global patterns of terrestrial vertebrate diversity and conservation. *Proceedings of the National Academy of Sciences* **110**, E2602-E2610 (2013).

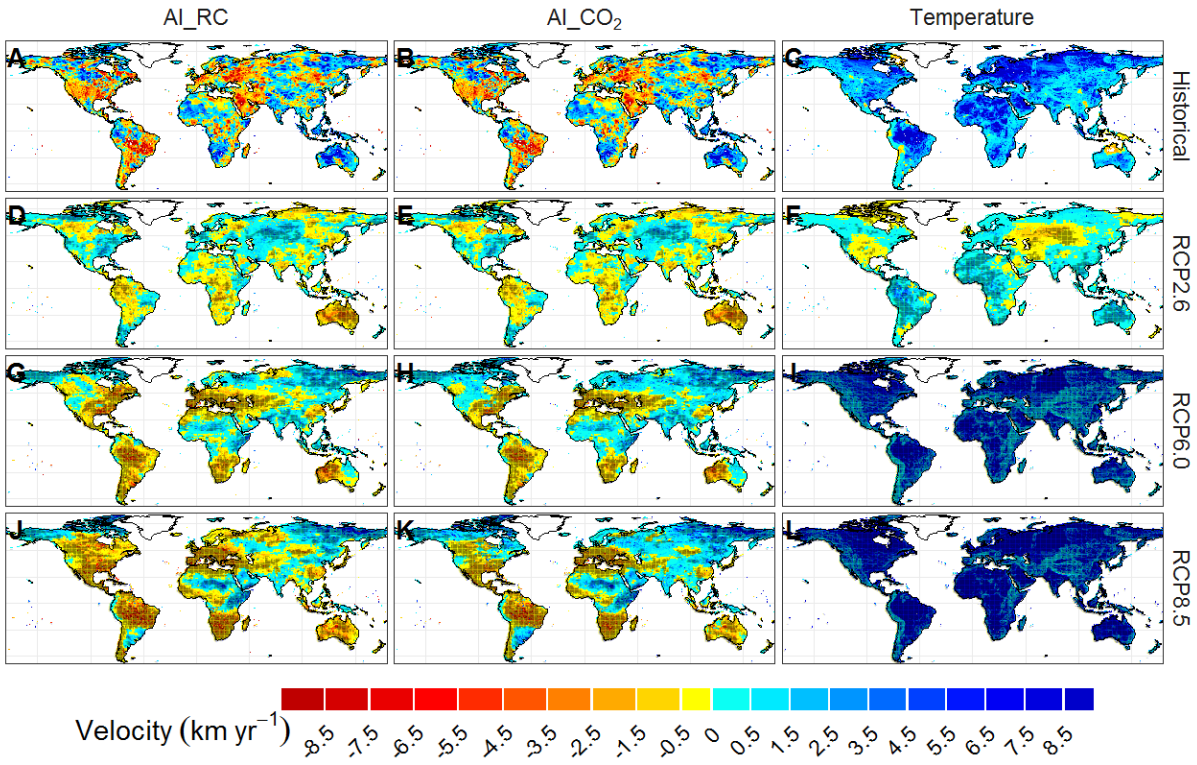


**Fig. 1. Speed maps of historical and future aridity and temperature velocities.** The negative sign of speed indicates drying/cooling and the positive sign indicating wetting/warming. The future speed values are the ensemble mean of multiple models. Pixels in each speed map with values outside the 0.5-99.5% quantiles are removed. All velocities are calculated by using the spatial gradient during 1979-2016. Stippling indicates the agreement in the sign of estimated velocities under RCPs across at least seven of nine models (75% of models). AI_RC refers to the aridity index based on the FAO reference crop potential evapotranspiration model and AI_$CO_2$ to one of its variants considering vegetation physiological responses to elevated $CO_2$.

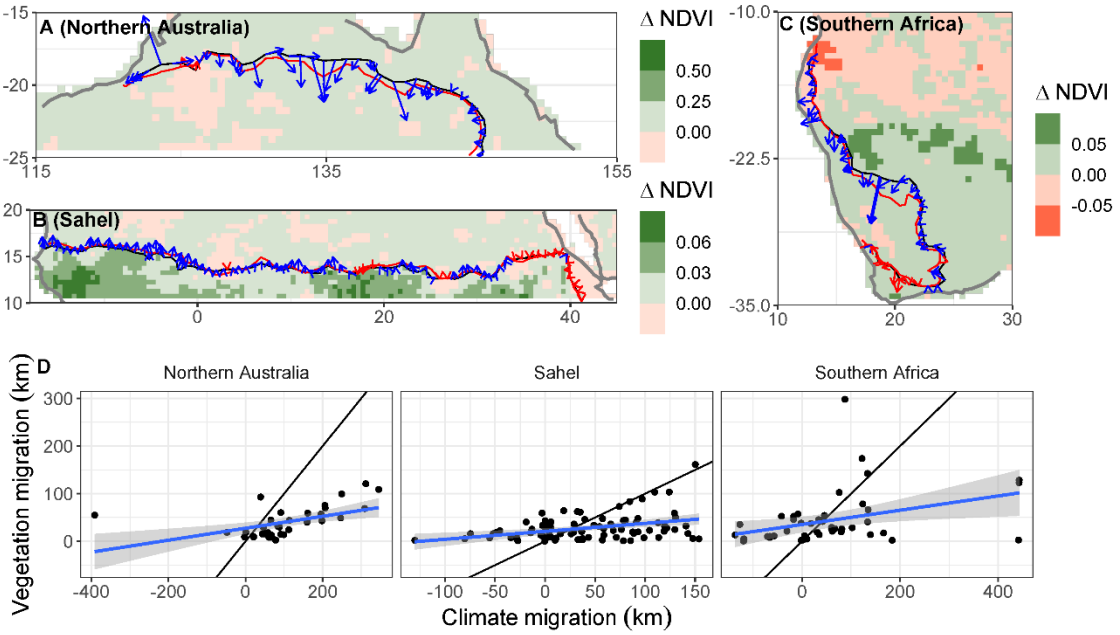


**Fig. 2. Coupling between aridity velocity (without considering $CO_2$ effects) and migration of NDVI isolines at multiple regions during 1982-2015. (*A*)** The migration of NDVI isolines (NDVI=0.30) in northern Australia during 1982-2015. **(*B*)** The migration of NDVI isolines (NDVI=0.20) in Sahel during 1982-2015. **(*C*)** The migration of NDVI isolines (NDVI=0.20) in southern Africa during 1982-2015. **(*A*-*C*)** The black and red lines denote NDVI isolines during 1982-1986 and during 2011-2015, respectively. The blue arrows indicate the directions of wetting velocity and the red arrows indicating directions of drying velocity. The length of arrows represents the migration distances of aridity velocity. The aridity velocities are calculated based on the spatial gradient during 1982-2015. The pixel values indicate the differences between NDVI during 1982-1986 and that during 2011-2015. **(*D*)** Correlations between migration distances of points along the NDVI isolines and the climate migration distances derived using the aridity velocity of these points. The black line is 1:1 line. All correlations are statistically significant with $r = 0.52$ & $p < 0.002$, $r = 0.37$ & $p < 0.001$, and $r = 0.36$ & $p < 0.015$, respectively.

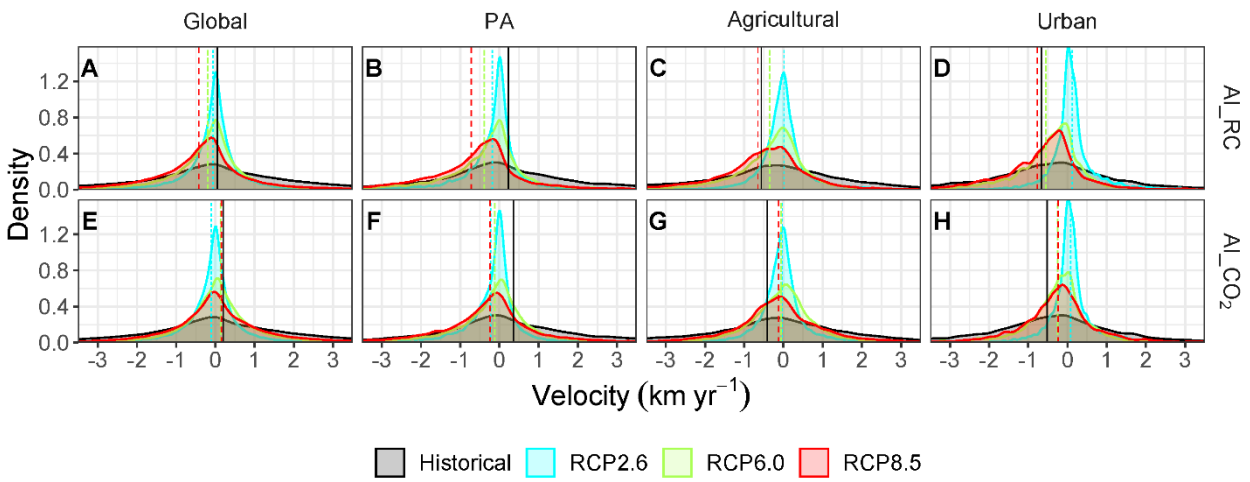


538
539 **Fig. 3. Probability density distribution of aridity velocity based on AI_RC or AI_$CO_2$ across**
540 **different land use types. (*A*-*D*)** Probability density distribution of speeds of aridity velocity for
541 the globe, protected areas (PA), agricultural areas, and urban areas. Negative values indicate drying
542 while the positive values indicating wetting. In each land use type, the two sample *t*-test is
543 conducted for aridity velocities under different scenarios and the results show they are all
544 significantly different ($p < 0.001$). AI_RC refers to the aridity index based on the FAO reference
545 crop potential evapotranspiration model and AI_$CO_2$ to one of its variants considering vegetation
546 physiological responses to elevated $CO_2$.
547
548
549
550
551
552
553
554
555
556
557

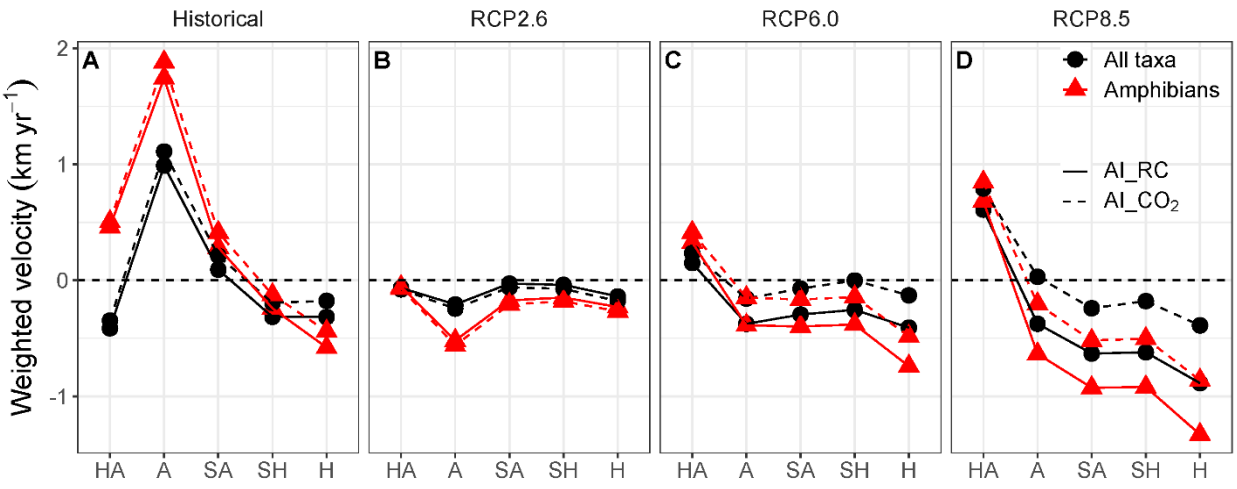


**Fig. 4. Aridity velocities for all taxa (amphibians, birds, mammals and plants) and amphibians under different scenarios.** The mean speed of aridity velocity for each taxon is weighted by grid area and species richness, in hyper-arid (HA), arid (A), semi-arid (SA), sub-humid (SH), and humid (H) regions. AI_RC refers to the aridity index based on the FAO reference crop potential evapotranspiration model and AI_$CO_2$ to one of its variants considering vegetation physiological responses to elevated $CO_2$.